Preclinical Characterization of Radioimmunoconjugate ^{111}In/^{90}Y-FF-21101 Against P-cadherin Expressing Tumor in Mouse Xenograft Model and Non-Human Primate

Yuichi Funase[1,2], Eri Nakamura[1], Masamichi Kajita[1], Yasutaka Saito[1], Shinobu Oshikiri[1], Michi Kitano[1], Masahiko Tokura[3], Akihiro Hino[1], and Tomoya Uehara[2]

[1]RI Research Department, *FUJIFILM Toyama Chemical Co., Ltd., Chiba, Japan*

[2]Graduate School of Pharmaceutical Sciences*, Chiba University, Chiba, Japan*

[3]Project Management Department, *FUJIFILM Toyama Chemical Co., Ltd., Tokyo, Japan*

Corresponding author:

Yuichi Funase

FUJIFILM Corporation, 577, Ushijima, Kaisei-machi, Ashigarakami-gun, Kanagawa 258-8577, Japan

Tel: +81-465-86-1732

Fax: +81-465-86-1224

E-mail: yuichi.funase@fujifilm.com

1

Word count: 6203

Running title: Anti-P-cadherin radioimmunotherapy

ABSTRACT

P-cadherin is overexpressed in various cancers and can be a target for radioimmunotherapy. We investigated the preclinical pharmacokinetics and pharmacology of FF-21101, an indium-111 (^{111}In)- or yttrium-90 (^{90}Y)-conjugated monoclonal antibody against P-cadherin, to evaluate its clinical applications.

Methods: The radiochemical purity, binding affinity, and *in vitro* serum stability of ^{111}In/^{90}Y-labeled FF-21101 were evaluated. The pharmacokinetics of ^{111}In/^{90}Y-FF-21101 were compared in normal mice. Tumor accumulation after ^{111}In-FF-21101 administration was investigated in mice bearing subcutaneous tumors with high (NCI-H1373), moderate (EBC-1), and negative (A549) P-cadherin expression. The tumor suppression effect following a single intravenous injection of ^{90}Y-FF-21101 was assessed in NCI-H1373 and EBC-1 mouse xenograft models. The relationship between antibody dose and tumor accumulation was investigated in the NCI-H1373 mouse xenograft model. The radiation-absorbed dose in humans after injection of ^{90}Y-FF-21101 was estimated using gamma camera images of cynomolgus monkeys.

Results: The radiochemical purities of [111]In- and ^{90}Y-FF-21101 were 98.2% ± 2.5% (n=9) and 99.3% ± 0.6% (n=5), respectively. The dissociation constant values were 1.083 nM for ^{111}In-FF-21101 and 1.367 nM for ^{90}Y-FF-21101. Both [111]In- and ^{90}Y-FF-21101 were stable in human serum after 96 h of incubation and exhibited similar pharmacokinetics in normal mice. The tumor accumulation of ^{111}In-FF-21101 was closely related to intensity of P-cadherin expression in the cells. ^{90}Y-FF-21101 showed significant tumor growth inhibition, implying NCI-H1373 and EBC-1 recurrence were not observed after the intravenous administration of ^{90}Y-FF-21101 3.7 and 7.4 MBq per animal, respectively. The tumor uptake in the mouse xenograft model and the estimated radiation-absorbed doses in the spleen of monkeys decreased with increasing antibody doses of ^{111}In-FF-21101. Conversely, the estimated radiation-absorbed dose in the red marrow increased with increasing antibody dose. An antibody dose of 4.8 mg/m^2 was considered appropriate for humans based on efficacy and safety. The estimated maximum tolerated radiation dose at this antibody dose was 2,886 MBq/human.

Conclusion: FF-21101 radioimmunotherapy exhibited high antitumor affinity and antitumor efficacy in mouse xenograft models. Extrapolation of the pharmacokinetics in monkeys to humans suggests the potential for clinical application of FF-21101 for treating P-cadherin expressing tumor.

Key Words: targeted radionuclide therapy, theranostics, CDH3, antibody, dosimetry

INTRODUCTION

P-cadherin, a cell-to-cell adhesion molecule, is overexpressed in several tumors, including breast, colon, lung, and pancreas (*1-3*) , and is implicated in tumor cell motility, migration, and invasiveness (*4*). P-cadherin is also involved in the epithelial–mesenchymal transition (*5*), cancer stem cell mediation (*6*), and breast cancer susceptibility gene mutations (*7*), and is associated with poor prognosis in various cancers (*2,8-11*). Conversely, P-cadherin expression levels are low in the normal tissues (*3*). Therefore, P-cadherin is considered to be an attractive target for solid tumor treatment. PF-03732010 is a humanized anti-P-cadherin monoclonal antibody (mAb) that exhibited high therapeutic efficacy in preclinical studies (*12*). However, PF-03732010 failed to exert therapeutic efficacy in the phase 1 trial (NCT00557505) (*13*), suggesting insufficient pharmacological activity for solid tumor treatment.

To enhance the pharmacological activity, we investigated yttrium-90 (^{90}Y)-conjugated anti-P-cadherin mAb, considering the successful therapeutic efficacy of ^{90}Y-ibritumomab tiuxetan, a ^{90}Y-labeled anti-CD20 antibody, against non-Hodgkin's lymphoma (*14*). Since P-cadherin expression is high in tumors and low in normal tissues; thus, it can facilitate appropriate biodistribution to achieve high efficacy with radioimmunotherapy. The phase 1 trial of PF-03732010 showed that a dosage of weekly 15 mg/kg body weight was well tolerated, suggesting that the unpredictable toxicity of anti-P-cadherin antibodies is unlikely.

FF-21101, a 1,4,7,10-tetraazacyclododecane-1,4,7,10-tetraacetic acid (DOTA)-conjugated chimeric human/mouse mAb of IgG$_1$ (PPMX2032), targets human P-cadherin. PPMX2032 has no anti-cell proliferation

activity. DOTA forms inert radiometal chelates with ^{111}In and [90]Y (15,16). The beta particles emitted from ^{90}Y induce cellular damage in target and neighboring cells via high-energy beta radiation and free radicals (17). ^{90}Y-FF-21101 constitutes an "armed antibody strategy" for solid tumor treatment and may be more effective than anti-P-cadherin therapy alone.

This study assessed the efficacy and safety of combining P-cadherin targeting and radionuclide therapy. We evaluated the tumor-suppressive effects of ^{90}Y-FF-21101, FF-21101, and ^{90}Y-labeled P-cadherin nonspecific antibody in a mouse xenograft model and estimated clinical safety of ^{90}Y-FF-21101 in humans by evaluating biodistribution in non-human primates, and then extrapolating those results to patients.

MATERIALS AND METHODS

Antibodies

PPMX2032 and FF-21101 were obtained from Perseus Proteomics Inc. (Tokyo, Japan) and FUJIFILM Diosynth Biotechnologies U.S.A. Inc. (Texas, USA).

Whole-molecule human IgG (hIgG) and S-2-(4-Isothiocyanatobenzyl)-1,4,7,10-tetraazacyclododecane tetraacetic acid (SCN-Bn-DOTA) were purchased from Thermo Fisher Scientific Inc. (Tokyo, Japan) and Macrocyclics Inc. (Texas, USA). hIgG was incubated with 50 mM bicine and 150 mM sodium chloride buffer (pH 8.5) containing SCN-Bn-DOTA for 17 h at 25°C. Purification of DOTA-conjugated hIgG (DOTA-hIgG) and buffer exchange with 250 mM sodium acetate (pH 5.5) were performed using PD-10 desalting columns (GE Healthcare, Illinois, USA).

Radiolabeling

FF-21101 and DOTA-hIgG were labeled with ^{111}In (^{111}InCl$_3$) (Nordion, Ontario, Canada) or ^{90}Y (^{90}YCl$_3$) (CIS Bio International, Saclay, France). The antibodies were incubated with ^{111}InCl$_3$ or ^{90}YCl$_3$ in 250 mM sodium acetate (pH 5.5) for 15 min at 45°C and purified using NAP-5 columns (GE Healthcare) with phosphate-buffered saline (PBS, pH 7.4). The radiochemical purities (>90%) were checked using Tec-Control Chromatography Strips 150–771 (BIODEX, New York, USA) developed with saline containing 10 mM diethylenetriaminepentaacetic acid. Non-labeled antibodies and/or PBS (pH 7.4) were used to adjust the protein concentration.

Binding Assay

The dissociation constants (Kds) of ^{111}In-FF-21101 and ^{90}Y-FF-21101 were evaluated with a saturation binding assay. sCDH3C (ECD1–ECD2 of human P-cadherin-mouse Fc fusion protein), an antigen of FF-21101, was obtained from Perseus Proteomics Inc. Eight-well strip plates, clear corner notched (Thermo Fisher Scientific, Massachusetts, USA), were treated with 250 µL/well of 1% glutaraldehyde solution at 37°C for 2 h. The plates were incubated with 100 µL/well of 20 µg/mL sCDH3 dissolved in 100 mM sodium acetate buffer at 25°C for 2 h with shaking and subsequent incubated overnight at 25°C. To determine non-specific binding, 100 mM sodium acetate buffer was added in the negative control wells. The plates were treated with 150 µL/well of 100 mM lysine sodium phosphate at 37°C for 1 h, followed by incubation with 200 µL/well of 10 mM calcium chloride containing 1% Block ace (KAC, Kyoto, Japan) at 37°C for 2 h with shaking. Radiolabeled FF-21101 (10 mg/mL) was diluted in

eight steps of two-fold serial dilution with 10 mM calcium chloride containing 0.4% Block ace. Each sample (100

μL/well) was added to the wells and incubated at 37°C for 3 h. Calcium chloride containing 0.1% Block ace (10

mM) was used as the washing buffer in each step. Radioactivity in each well and 100 μL of each serial dilution as a

total count were measured with a gamma counter. Kd and maximum binding (Bmax) values were calculated via

nonlinear regression using GraphPad Prism Version 5.04 software (GraphPad Software, California, USA) [one

site-binding analysis equation $Y = Bmax \times X / (Kd + X)$].

In Vitro Stability in Serum

^{111}In-FF-21101 and ^{90}Y-FF-21101 were added to human serum (Access Biologicals, California, USA) at a

concentration of 0.5 MBq/5 μg/mL (n=3). The methodology is described in Supplemental Method 1 (*18-20*). The

serum samples were analyzed after incubation for 0, 3, 24, 48, and 96 h at 37°C using sodium dodecyl sulfate

poly-acrylamide gel electrophoresis. The mixture of each sample and 100 mM DTPA at 9:1 was mixed with an equal

amount of Novex Tris-Glycine SDS Sample Buffer (Thermo Fisher Scientific) and heated at 85°C for 2 minutes.

Electrophoresis was performed using Novex 4%–20% Tris-Glycine Mini Gels and Novex Tris-Glycine SDS

Running Buffer (Thermo Fisher Scientific). The electrophoresed gels were exposed to BAS IP (GE Healthcare) in a

freezer set at −20°C. BAS IP was measured for radioactivity using Typhoon FLA 7000IP (GE Healthcare); the

resultant images were analyzed with Multi Gauge (FUJIFILM, Tokyo, Japan). Data were normalized to 100% at t =

0.

Animal Studies

All animal studies were performed in accordance with the Institutional Animal Care and Use Committee

of FUJIFILM Toyama Chemical Co., Ltd., and adhered to the Guidelines for Proper Conduct of Animal

Experiments issued by the Science Council of Japan (June 1, 2006).

Comparative Biodistribution of ^{111}In-FF21101 and ^{90}Y-FF-21101 in Normal Mice

Eight-week-old BALB/c mice (Charles River Laboratories Japan, Kanagawa, Japan) were stratified based

on body weight and randomly assigned to 10 groups (five mice/group) using the statistical analysis software EXSUS

(CAC Croit Corporation, Tokyo, Japan). The mice were intravenously administered 0.5 MBq/40 μg ^{111}In-FF-21101

(five groups) or ^{90}Y-FF-21101 (five groups). At 5 min and 24, 48, 96, and 192 h after administration, the blood, heart,

lungs, liver, kidneys, spleen, and bones were removed and weighed. Non-bone tissues were dissolved in

SOLVABLE (PerkinElmer, Massachusetts, USA) overnight at 50°C under shaking conditions; bones were dissolved

in hydrochloric acid overnight at 37°C under shaking conditions. The dissolved tissue fluids were examined for

radioactivity; the tissue radioactivity level, expressed as percent of administered activity remaining in a tissue

(%ID/g), was calculated from the weights and radioactivity levels of the collected tissues. PK parameters were

estimated from each time point as mean %ID/g of blood using the WinNonlin pharmacokinetic software (CERTARA,

New Jersey, USA) with the non-compartmental approach.

Cell Culture

Human lung adenocarcinoma cell lines, NCI-H1373 and A549, were purchased from the American Type Culture Collection (Virginia, USA). The human lung squamous cell carcinoma cell line, EBC-1, was purchased from the Japanese Collection of Research Bioresources Cell Bank (Oosaka, Japan). NCI-H1373, EBC-1, and A549 were selected as high-, moderate-, and non-P-cadherin-expression cell lines, respectively (*21*). The following cell culture media, containing 10% fetal bovine serum (Moregate Biotech, Queensland, Australia) and 1% penicillin/streptomycin (Thermo Fisher Scientific) were used: minimum essential media (Thermo Fisher Scientific) for EBC-1, Roswell Park Memorial Institute 1640 media (Thermo Fisher Scientific) for NCI-H1373, and Ham's F-12K (Kaighn's) media (Thermo Fisher Scientific) for A549. The cultures were maintained at 37°C under a humidified atmosphere (5% CO_2).

Mouse Xenograft Model

Male BALB/c Slc-nu/nu mice [7-8 weeks old (Japan SLC, Shizuoka, Japan)] were subcutaneously inoculated with 5×10^6 cells/0.1 mL NCI-H1373, EBC-1, or A549 suspended in Dulbecco's PBS in the right flank. One to two weeks after transplantation (until the mean tumor volume reached approximately 200 mm^3), the mice were randomized on the basis of tumor volume and body weight to different groups, using the statistical analysis software EXSUS. The tumor volume was calculated as long diameter × (short diameter)^2 / 2.

Biodistribution in Mouse Xenograft Models

^{111}In-FF-21101 or ^{111}In labeled DOTA-hIgG (^{111}In-hIgG) of 740 kBq/30 μg was administered to the

NCI-H1373, EBC-1, and A549 mouse xenograft models via the tail vein. The mice were euthanized by

exsanguination under anesthesia at 5 min and at 24, 48, 96, and 192 h after administration (n=3 per time point). All

organs of interest (blood, brain, heart, lungs, liver, spleen, pancreas, stomach, small intestine, cecum, large intestine,

kidneys, adrenals, adipose, testes, bone, muscle, skin, thyroid, and tumor) were removed. The tissue weights and the

radioactivity were measured.

In Vivo Efficacy

We estimated the therapeutic efficacy of ^{90}Y-FF-21101 as follows. On day 0, the NCI-H1373- and EBC-1

mouse xenograft models were assigned to the following four groups (n = 6/group): 1) single administration of PBS;

2) administration of 10 mg/kg PPMX2032 twice a week for 3 weeks; 3) single administration of 3.7 MBq/30 μg

^{90}Y-FF-21101; and 4) single administration of 3.7 MBq/30 μg ^{90}Y-labeled DOTA- hIgG (^{90}Y-hIgG).

A radiation dose-escalation study was also performed. On day 0, the EBC-1 mouse xenograft model was

assigned to the following three groups (n = 6/group): 1) single administration of PBS; 2) single administration of 3.7

MBq/30 μg ^{90}Y-FF-21101; and 3) single administration of 7.4 MBq/30 μg ^{90}Y-FF-21101.

The injectates were administered from day 1 to each mouse via the tail vein. The tumor volume and the

body weight were measured twice a week. The mice were euthanized when their body weight decreased to >20% of

that at day 0 or if the tumor volume exceeded 10% of the total body weight. The time point at which individual mice

were euthanized was defined as the end point of the group.

Antibody Dose Optimization in Mouse Xenograft Model

^{111}In-FF-21101 was administered at 740 kBq/3.73, /30, /112, or /373 μg to NCI-H1373-inoculated mice

via the tail vein. The mice were euthanized by exsanguination under anesthesia at 5 min and at 24, 48, 96, and 192 h

after administration (n=3 per time point), and the weight and radioactivity of the extirpated tumor were measured.

Biodistribution and Dosimetry in Cynomolgus Monkeys

This study was conducted in three adult cynomolgus monkeys (HAMRI, Ibaraki, Japan), following

^{111}In-FF-21101 bolus intravenous administration. The monkeys were administered approximately 37 MBq/kg

^{111}In-FF-21101 at an antibody dose of 0.04, 0.4, or 4 mg/kg, respectively. Blood samples were collected by

venipuncture at 0.17, 0.5, 1, 3, 6, 24, 48, 72, 96 (or 120), 144, 168, and 216 h following the administration. The

radioactivity of the blood samples and the counting standards (diluted administered solution) were measured using a

gamma counter to calculate %ID/mL of blood.

$$\%\text{ID/mL of blood} = \frac{\text{Radioactivity of blood (cpm/mL)}}{\text{Administered activity (cpm)}} \times 100$$

Administered activity (cpm)

$$= \text{Counting standard activity (cpm)} \times \text{Dilution factor} \times \frac{\text{Administered volume (mL)}}{\text{Counting standard volume (mL)}}$$

Based on the %ID/mL values of the blood, the biological pharmacokinetic parameters were estimated using the WinNonlin pharmacokinetic software with the non-compartmental approach consistent with the IV bolus route of administration. All parameters were generated from the scaled %ID/mL of blood.

$$\text{Scaled \%ID/mL} = \frac{\text{\%ID}}{\text{Max \%ID}} \times 100$$

Max %ID = Maximum value of %ID × Monkey blood volume (mL)

Monkey blood volume (mL) = Monkey body weight (kg) × Monkey circulating blood volume (mL/kg)

Monkey circulating blood volume: 65 mL/kg (*22*)

Each monkey was administered general anesthesia and underwent whole-body planar scintigraphy with a calibration source (diluted administered solution) at 3, 6, 24, 48, 72, 96 (or 120), 144, and 168 h after administration using Symbia E (SIEMENS, Tokyo Japan). Radioactivity of the calibration source was measured using a gamma counter to calculate ratio of calibration source.

$$\text{Ratio of calibration source} = \frac{\text{Calibration source activity (cpm)}}{\text{Administered activity (cpm)}}$$

The acquisition parameters were set as follows; matrix size was 256×512, scan speed was 5 cm/min (until

48 h post administration) or 3 cm/min (after 72 h post administration), and energy window was set to 15% window

for both 173 keV and 247 keV. The scanner was configured with a medium-energy low-penetration collimator for

the data acquisition. A region of interest (ROI) was set for the detectable organs; each ROI count was calculated

using the syngo® MI Application VA60C (SIEMENS). Tissue %ID, the percent of administered activity remaining in

a tissue, was calculated from each ROI count. The ROI of background (BG) were set the four corners of the field of

view in each the anterior and the posterior images. The ROI of body background (BBG) were set 8 locations at

muscle part in each of the anterior and the posterior whole body images. The count per pixel (CPP) of the BG and

the BBG were calculated for each of the anterior and the posterior images. The ROI of the calibration source, whole

body, heart, liver, spleen, and lungs were set along the shapes of the accumulations. The count of the calibration

source, the whole body and the each organ were calculated in each the anterior and the posterior images.

Count of calibration source $=$ ROI count of calibration source $-$ CPP of BG $\times$ ROI size of calibration source

Count of whole body $=$ ROI count of whole body $-$ CPP of BG $\times$ ROI size of whole body

Count of organ $=$ ROI count of organ $-$ CPP of BBG $\times$ ROI size of organ

The count of the anterior and the posterior each ROI were averaged and used for calculation of %ID.

$$\%\text{ID of whole body} = \frac{\text{Averaged count of whole body}}{\text{Administered count}} \times 100$$

$$\%\text{ID of organ} = \frac{\text{Averaged count of organ}}{\text{Administered count}} \times 100$$

$$\text{Administered count} = \frac{\text{Averaged count of calibration source}}{\text{Ratio of calibration source}}$$

The time-integrated activity coefficients of red marrow were calculated from blood radioactivity. The %ID/mL in the blood of each time point was converted to the fraction of administered activity per mL (FIA/mL). FIA/mL values were performed decay correction, humanization, and scaling that the maximum value of FIA (Max FIA) would be 1.0. These calculations are shown in below. The half-life of ^{90}Y was used 64 hours.

$$\text{Scaled FIA/mL} = \frac{\text{Humanized FIA/mL}}{\text{Humanized Max FIA}}$$

$$\text{Humanized FIA/mL} = \text{Decay corrected FIA/mL} \times \frac{\text{Monkey body mass}}{\text{Reference body mass}}$$

Reference body mass (male): 73700 g (default value of OLINDA/EXM 1.0)

$$\text{Humanized Max FIA} = \text{Maximum value of Humanized FIA/mL} \times \text{Reference blood volume}$$

Reference blood volume (male): 5300 mL (*19*)

$$\text{Decay corrected FIA/mL} = \text{FIA/mL} \times 0.5^{(t\,/\,\text{half life})}$$

$$\text{FIA/mL} = \frac{\%\text{ID/mL}}{100}$$

Scaled FIA/mL values were performed Non-compartmental analysis with WinNonlin to calculate the time-integrated activity coefficients of the blood ($T_{blood/mL}$). The time-integrated activity coefficients of the red marrow ($T_{redmarrow}$) were calculated according to the formula (23).

$$T_{redmarrow} = T_{blood/mL} \times \text{Reference red marrow mass} \times \frac{RMECFF}{1 - HCT}$$

Reference red marrow mass (male): 1120 g (default value of OLINDA/EXM 1.0)

RMECFF (Red marrow extracellular fluid fraction): 0.19 (24)

HCT (Hematocrit): 0.47

We calculated the time-integrated activity coefficients for the monkey from planar imaging by plotting and integrating the measured effective activities for each imaged source organ over some number of time points. The %ID of each ROI was converted to the fraction of injected activity (FIA = %ID / 100). The FIA values were performed Non-compartmental analysis with WinNonlin to calculate the time-integrated activity coefficients of the organ (T_{organ}). The time-integrated activity coefficients of the remainder were calculated by subtracting the time-integrated activity coefficients of other tissues from that of the whole body. The absorbed dose estimates were computed using OLINDA/EXM 1.0 (Hermes Medical Solutions, North Carolina, USA) from the time-integrated activity coefficients of the each organ. Source organs were red marrow, heart contents, liver, lungs, spleen, and remainder of body. A nuclide was used ^{90}Y. A reference model was selected the Adult Male.

Statistical Analyses

Statistical analyses were performed using the statistical analysis software EXSUS. Significance was determined using the Steel–Dwass test at day 22 (NCI-H1373) and day 18 (EBC-1) for comparing the tumor volume between the PBS-, PPMX2032-, ^{90}Y-hIgG- (3.7 MBq/animal), and ^{90}Y-FF-21101- (3.7 MBq/animal) administration groups. P-values <0.05 were considered statistically significant. Data were presented as mean ± SD.

RESULTS

Radiolabeling, Binding Activity, and Serum Stability In Vitro

The radiochemical purities (mean ± SD) of ^{111}In-FF-21101, ^{90}Y-FF-21101, ^{111}In-hIgG, and ^{90}Y-hIgG were 98.2% ± 2.5% [91.6–99.9% (n=9)], 99.3% ± 0.6% [98.2–99.7% (n=5)], 99.4% ± 0.3% [99.2–99.6 (n=2)], and 99.2% ± 0.6% [98.7–99.6% (n=2)], respectively. The Kds of ^{111}In-FF-21101 and ^{90}Y-FF-21101 were 1.083 and 1.367 nM, respectively (Figure 1). Both ^{111}In-FF-21101 and ^{90}Y-FF-21101 remained stable in serum for 96 h (Table 1).

Comparative Pharmacokinetics of ^{111}In/^{90}Y-FF-21101 in Normal Mice

^{90}Y-FF-21101 and ^{111}In-FF-21101 displayed similar pharmacokinetics. The radioactivity in the blood of ^{90}Y-FF-21101 and ^{111}In-FF-21101 registered the highest values 5 min after administration (35.3 and 35.9 %ID/g, respectively). Both ^{90}Y-FF-21101 and ^{111}In-FF-21101 exhibited similar PK parameters (Table 2) and the %ID/g versus time for each organ (Figure 2).

Antigen-Specific Tumor Accumulation

^{111}In-FF-21101 showed antigen-specific tumor accumulation (Figure 3A). The maximum ^{111}In-FF-21101 tumor uptakes were 48.2 and 30.7 %ID/g in the NCI-H1373 and EBC-1 mouse xenograft models, respectively. Conversely, ^{111}In-hIgG tumor accumulation was insignificant; the maximum tumor uptakes were 9.7 and 11.3 %ID/g in the NCI-H1373 and EBC-1 mouse xenograft model, respectively. ^{111}In-FF-21101 and ^{111}In-hIgG, tumor accumulation in the A549 mouse xenograft model was also insignificant, with maximum tumor uptakes of 8.1 and 6.0 %ID/g, respectively. When tumor accumulation was low, blood radioactivity was high (Figure 3B). P-cadherin-specific and nonspecific antibody accumulations in other tissues were insignificant and there were no major differences between the models (Supplemental Tables 1–6).

Tumor Suppressive Effects

The mean tumor volumes at day 0 in the NCI-H1373 and EBC-1 mouse xenograft models were 191 and 277 mm^3, respectively. No animals lost >20% of their body weight. The body weight did not differ between groups (Supplemental Figures 1, 2). ^{90}Y-FF-21101 exhibited the strongest tumor suppressive effect in the two xenograft models (Figures 4A, 4B). Conversely, PPMX2032 and ^{90}Y-hIgG did not show significant differences against PBS in either model. Although ^{90}Y-FF-21101 (3.7 MBq/animal) showed a high antitumor effect, tumor regrowth was observed in the EBC-1 model from day 22. Therefore, a radiation dose-escalation therapeutic study was conducted in the EBC-1 mouse xenograft model. The mean tumor volume at day 0 was 197 mm^3 and tumor regrowth was not

observed in the ^{90}Y-FF-21101 (7.4 MBq/animal) group until day 74 (Figure 5A). Complete tumor regression was observed in five mice in the ^{90}Y-FF-21101 (7.4 MBq/animal) group. Although transient weight loss was observed in the ^{90}Y-FF-21101 (7.4 MBq) group on days 5–15, no animals lost >20% body weight until day 74 (Figure 5B).

Effect of Antibody Dose on Tumor Accumulation in Mouse Xenograft Model, Pharmacokinetics in Cynomolgus Monkeys, and Estimated Radiation-Absorbed Dose in Humans

The tumor uptake in NCI-H1373-inoculated mice of ^{111}In-FF-21101 decreased with increases in antibody dose and the trend persisted at each time point (Figure 6A).

In cynomolgus monkeys, approximately 70–80% of the administered activity of ^{111}In-FF-21101 was found throughout the body 3 h post injection; radioactivity counts decreased to approximately 50%–60% at 168 h post injection. The accumulation of ^{111}In-FF-21101 in the heart, liver, spleen, and the lungs were 7–9, 10–12, 1–5, and 4–6 %ID at 3 h post injection, respectively. The radioactivity in the heart and lungs decreased to <40% at 168 h post-infusion, with a slightly longer retention of radioactivity in the spleen and liver at 168 h post-infusion. The radioactivity levels in the spleen decreased and those in the heart increased with increasing antibody dose (Figure 6B). The blood showed peak radioactivity levels at 10 min post injection of ^{111}In-FF-21101. The area under the curve and biological half-life ($T_{1/2}$) values increased and clearance values decreased with increasing antibody dose level. No remarkable trends in the maximum concentration and volume of distribution at steady state (V_{ss}) values among the antibody dose levels (Table 3).

The estimated radiation-absorbed doses of ^{90}Y-FF-21101 in humans were extrapolated from the results of monkeys (Table 4). Increased antibody dose significantly lowered the estimated radiation-absorbed dose of ^{90}Y-FF-21101 in the spleen. The estimated radiation-absorbed dose slightly increased with increased antibody dose in the heart wall, red marrow, osteogenic cells, and whole body.

DISCUSSION

Other than PF-03732010, tumor treatment targeting P-cadherin such as PF-06671008 (bispecific antibody against P-cadherin and CD3) (*25*) and PCA-062 (DM1 conjugated antibody) (NCT02375958) were challenged. We chose a targeted radionuclide therapy approach using β-emitters based on the success of ^{90}Y-ibritumomab tiuxetan (*14*) and ^{177}Lu-DOTATATE (*26*). For application of ^{90}Y-FF-21101 to clinical studies, here we showed that ^{90}Y-FF-21101 could expose tumors to radioactivity required for treatment without serious radiotoxicity in normal tissues.

^{111}In- and ^{90}Y-FF-21101 showed robustness of radiolabeling, remained stable in human serum, and exhibited similar P-cadherin binding affinities and biodistribution; thus, ^{111}In-FF-21101 could be used to estimate ^{90}Y-FF-21101 pharmacokinetics.

^{111}In-FF-21101 and ^{111}In-hIgG were administered to mouse xenograft models with different levels of P-cadherin expression (high: NCI-H1373, moderate: EBC-1, negative: A549) (*21*); we found that ^{111}In-FF-21101 accumulation in tumors was dependent on P-cadherin expression levels. ^{111}In-FF-21101 tumor accumulation in A549

was unrelated to antigen specificity because it was as low as ^{111}In-hIgG tumor accumulation. Furthermore, ^{111}In-hIgG accumulation in P-cadherin-positive cells was as low as that in P-cadherin-negative cells and lower than that in the blood (Figures 3A, 3B). Therefore, differences in ^{111}In-FF-21101 accumulation in the tumor of different P-cadherin expression levels supported the P-cadherin-specific accumulation of ^{111}In-FF-21101.

The biodistribution profiles of ^{111}In-FF-21101 were well reflected in the suppressed tumor growth of the P-cadherin-positive xenografted tumor cells following ^{90}Y-FF-21101 administration. The single injection of 3.7 MBq ^{90}Y-FF-21101 significantly suppressed tumor growth compared with the PBS-, PPMX2032-, and ^{90}Y-hIgG-treated groups. The difference in the tumor suppression period between the two models reflected different tumor accumulation based on P-cadherin expression levels. Tumor regrowth was not observed in 7.4 MBq/animal ^{90}Y-FF-21101 administered EBC-1 mouse xenograft model up to day 74. Therefore, it was predicted that radioactivity equivalent to at least 7.4 MBq/mouse was required in humans for obtaining a high antitumor effect in clinical.

The effect of antibody dose on ^{111}In-FF-21101 biodistribution was investigated to estimate the clinical dose. The tumor uptake in mouse xenograft model of ^{111}In-FF-21101 decreased with an increasing antibody dose, indicating that the FF-21101-binding sites on the tumor cells get saturated at high antibody doses. FF-21101 has no cross-reactivity with mouse P-cadherin; we studied PK and dosimetry using cynomolgus monkeys with reactive antigens for FF-21101. Furthermore, serum soluble P-cadherin levels in cynomolgus monkeys are similar to healthy humans and cancer patients (27). The radiation-absorbed dose increased in the organs affected by blood flow such as

the red marrow and heart, because of prolonged radioactivity retention in the blood with antibody dose increases. The radiation-absorbed dose to the spleen decreased with an increase in antibody dose (Table 4). A similar phenomenon was observed in ^{111}In-ibritumomab tiuxetan with pre-administration of unlabeled anti-CD20 antibodies in humans (28). Thus, the antibody dose optimization should consider both tumor accumulation and normal tissue distribution.

Based on results from monkeys and mice, we estimated the clinical antibody doses of ^{90}Y-FF-21101. Because the antibody dose of FF-21101 in clinical study will be based on body surface area, the antibody doses (mg/kg) for the cynomolgus monkey were converted to dosage based on body surface area (mg/m^2). The dosage was converted to dose per individual (μg/animal) for mice [Table 5 (Supplemental Method 2) (29)]. The upper limits of the radiation-absorbed dose were set at 3,000 mGy and 20,000 mGy for the red marrow and any other organ, respectively (30), and the dose-limiting organ and maximum radiation dose were estimated at each antibody dose (Table 6). A radiation dose of 7.4 MBq/animal in the mouse xenograft model corresponded to 888 MBq/m^2 and 1,678 MBq/human (Supplemental Method 3) (18,19,29). An antibody dose of 0.48 mg/m^2 (1,667 MBq/human as maximum radiation dose) would result in an inadequate margin of safety for a therapeutic radiation dose of 1,678 MBq/human. Dose-limiting organ at 48 mg/m^2 was red marrow linked to a high radiotoxicity risk. Furthermore, 48 mg/m^2 (equivalent to 400 μg/animal in mice) was higher than 378 μg/animal in mice as an antibody dose, suggesting that tumor accumulation was insufficient (Figure 6A). Based on our calculations, an antibody dose of 4.8 mg/m^2 for ^{90}Y-FF-21101 was estimated as appropriate for humans. Because the 4.8 mg/m^2 [0.13 mg/kg in humans

(Supplemental Method 4) (*29*)] was much lower than that of PF-03732010 (15 mg/kg), for which toxicity was not observed in the phase 1 trial (*13*), the risk of toxicity derived from antibodies would also be low. Moreover, the 4.8 mg/m^2 enables administration of up to 2,886 MBq/human, which is markedly higher than the estimated therapeutic radiation dose (1,678 MBq/human).

CONCLUSION

^{111}In-FF-21101 showed P-cadherin-specific high tumor accumulation and ^{90}Y-FF-21101 significantly suppressed P-cadherin-expressing tumors. Analysis of the estimated radiation-absorbed dose of ^{90}Y-FF-21101 in humans predicted the antibody and radiation dose in clinical cases and showed sufficient safety. Therefore, promising outcomes can be expected for a clinical trial with FF-21101. It is reasonable to estimate the radiation-absorbed dose of ^{90}Y-FF-21101 using ^{111}In-FF-21101 due to similar biodistributions and PKs demonstrated both *in vivo*. Based on these findings, a phase 1 trial in the U.S.A. (NCT02454010) was conducted using an antibody dose from 0.625 to 3.125 mg/m^2. The expansion phase is performed with an antibody dose of 3.125 mg/m^2.

DISCLOSURE

ACKNOWLEDGMENTS

KEY POINTS

QUESTION: Is the clinical application of P-cadherin radioimmunotherapy promising?

PERTINENT FINDINGS: P-cadherin radioimmunotherapy demonstrated a significantly higher antitumor effect than anti-P-cadherin antibody monotherapy and P-cadherin nonspecific radioimmunotherapy in a mouse xenograft model. Based on the radiation-absorbed dose analysis, ^{90}Y-FF-21101 was estimated to be capable of administering sufficiently high radioactivity compared with the estimated radioactivity required for human treatment.

IMPLICATIONS FOR PATIENT CARE: Combining ^{90}Y with P-cadherin specific antibody may be a possible

therapeutic strategy for P-cadherin-expressing cancer.

REFERENCES

1.   Xi L, Feber A, Gupta V, et al. Whole genome exon arrays identify differential expression of alternatively spliced, cancer-related genes in lung cancer. *Nucleic Acids Res.* 2008;36:6535-6547.

2.   Paredes J, Albergaria A, Oliveira JT, Jeronimo C, Milanezi F, Schmitt FC. P-cadherin overexpression is an indicator of clinical outcome in invasive breast carcinomas and is associated with CDH3 promoter hypomethylation. *Clin Cancer Res.* 2005;11:5869-5877.

3.   Imai K, Hirata S, Irie A, et al. Identification of a novel tumor-associated antigen, cadherin 3/P-cadherin, as a possible target for immunotherapy of pancreatic, gastric, and colorectal cancers. *Clin Cancer Res.* 2008;14:6487-6495.

4.   Ribeiro AS, Albergaria A, Sousa B, et al. Extracellular cleavage and shedding of P-cadherin: a mechanism underlying the invasive behaviour of breast cancer cells. *Oncogene.* 2010;29:392-402.

5.   Ribeiro AS, Paredes J. P-Cadherin linking breast cancer stem cells and invasion: a promising marker to identify an "intermediate/metastable" EMT state. *Front Oncol.* 2014;4:371.

6.   Vieira AF, Ricardo S, Ablett MP, et al. P-cadherin is coexpressed with CD44 and CD49f and mediates stem cell properties in basal-like breast cancer. *Stem Cells.* 2012;30:854-864.

7.   Warmoes M, Lam SW, van der Groep P, et al. Secretome proteomics reveals candidate non-invasive biomarkers of BRCA1 deficiency in breast cancer. *Oncotarget.* 2016;7:63537-63548.

8.   Imai S, Kobayashi M, Takasaki C, Ishibashi H, Okubo K. High expression of P-cadherin is significantly associated with poor prognosis in patients with non-small-cell lung cancer. *Lung Cancer.* 2018;118:13-19.

9.   Sun L, Hu H, Peng L, et al. P-cadherin promotes liver metastasis and is associated with poor prognosis in colon cancer. *Am J Pathol.* 2011;179:380-390.

10.   Sakamoto K, Imai K, Higashi T, et al. Significance of P-cadherin overexpression and possible mechanism of its regulation in intrahepatic cholangiocarcinoma and pancreatic cancer. *Cancer Sci.* 2015;106:1153-1162.

11.   Tothill RW, Tinker AV, George J, et al. Novel molecular subtypes of serous and endometrioid ovarian cancer linked to clinical outcome. *Clin Cancer Res.* 2008;14:5198-5208.

12.   Zhang CC, Yan Z, Zhang Q, et al. PF-03732010: a fully human monoclonal antibody against P-cadherin with antitumor and antimetastatic activity. *Clin Cancer Res.* 2010;16:5177-5188.

13.   Vieira AF, Paredes J. P-cadherin and the journey to cancer metastasis. *Mol Cancer.* 2015;14:178.

14.   Witzig TE, Flinn IW, Gordon LI, et al. Treatment with ibritumomab tiuxetan radioimmunotherapy in patients with rituximab-refractory follicular non-Hodgkin's lymphoma. *J Clin Oncol.* 2002;20:3262-3269.

15.   Gholipour N, Jalilian AR, Khalaj A, et al. Preparation and radiolabeling of a lyophilized (kit) formulation of DOTA-rituximab with ^{90}Y and ^{111}In for domestic radioimmunotherapy and radioscintigraphy of non-Hodgkin's lymphoma. *Daru.* 2014;22:58.

16.   Griffiths GL, Govindan SV, Sharkey RM, Fisher DR, Goldenberg DM. 90Y-DOTA-hLL2: an agent for radioimmunotherapy of non-Hodgkin's lymphoma. *J Nucl Med.* 2003;44:77-84.

17.   Matsumoto K, Okajo A, Kobayashi T, Mitchell JB, Krishna MC, Endo K. Estimation of free radical formation by beta-ray irradiation in rat liver. *J Biochem Biophys Methods.* 2005;63:79-90.

18.   Du Bois D, Du Bois EF. A formula to estimate the approximate surface area if height and weight be known. 1916. *Nutrition.* 1989;5:303-311; discussion 312-303.

19.   Protection ICoR. Basic anatomical and physiological data for use in radiological protection reference values. *ICRP Publication 89.* 2002;32:5-265.

20.   Feldschuh J, Enson Y. Prediction of the normal blood volume. Relation of blood volume to body habitus. *Circulation.* 1977;56:605-612.

21.   Yoshioka H, Yamamoto S, Hanaoka H, et al. In vivo therapeutic effect of CDH3/P-cadherin-targeting radioimmunotherapy. *Cancer Immunol Immunother.* 2012;61:1211-1220.

22.   Diehl KH, Hull R, Morton D, et al. A good practice guide to the administration of substances

and removal of blood, including routes and volumes. *J Appl Toxicol.* 2001;21:15-23.

23.   Wessels BW, Bolch WE, Bouchet LG, et al. Bone marrow dosimetry using blood-based models for radiolabeled antibody therapy: a multiinstitutional comparison. *J Nucl Med.* 2004;45:1725-1733.

24.   Sgouros G. Bone marrow dosimetry for radioimmunotherapy: theoretical considerations. *J Nucl Med.* 1993;34:689-694.

25.   Root AR, Cao W, Li B, et al. Development of PF-06671008, a highly potent anti-P-cadherin/anti-CD3 bispecific DART molecule with extended half-life for the treatment of cancer. *Antibodies (Basel).* 2016;5.

26.   Strosberg J, El-Haddad G, Wolin E, et al. Phase 3 trial of (177)Lu-dotatate for midgut neuroendocrine tumors. *N Engl J Med.* 2017;376:125-135.

27.   Betts A, Haddish-Berhane N, Shah DK, et al. A translational quantitative systems pharmacology model for CD3 bispecific molecules: application to quantify T cell-mediated tumor cell killing by P-cadherin LP DART((R)). *Aaps j.* 2019;21:66.

28.   Knox SJ, Goris ML, Trisler K, et al. Yttrium-90-labeled anti-CD20 monoclonal antibody therapy of recurrent B-cell lymphoma. *Clin Cancer Res.* 1996;2:457-470.

29.   Nair AB, Jacob S. A simple practice guide for dose conversion between animals and human. *J Basic Clin Pharm.* 2016;7:27-31.

30.   Wiseman GA, White CA, Sparks RB, et al. Biodistribution and dosimetry results from a phase III prospectively randomized controlled trial of Zevalin radioimmunotherapy for low-grade, follicular, or transformed B-cell non-Hodgkin's lymphoma. *Crit Rev Oncol Hematol.* 2001;39:181-194.
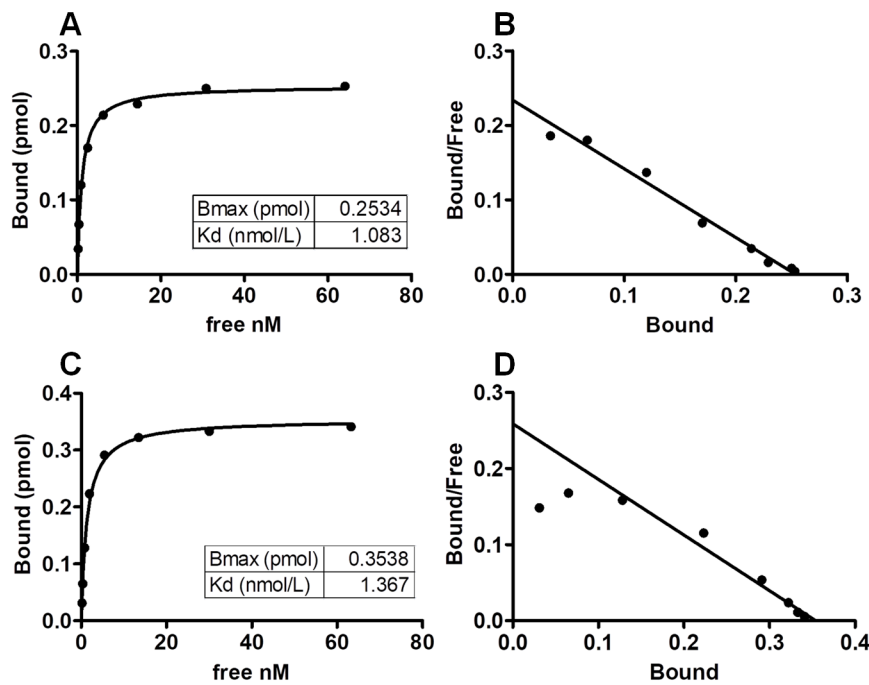
FIGURE 1. Binding activity of radiolabeled FF-21101 to sCDH3C

(A) Saturation binding curve of ^{111}In-FF-21101, (B) Scatchard plot of ^{111}In-FF-21101, (C) saturation binding curve of ^{90}Y-FF-21101, and (D) Scatchard plot of ^{90}Y-FF-21101. "Bound" refers to the amount of radiolabeled FF-21101 bound to sCDH3C. "Free" refers to the concentration of free radiolabeled FF-21101.
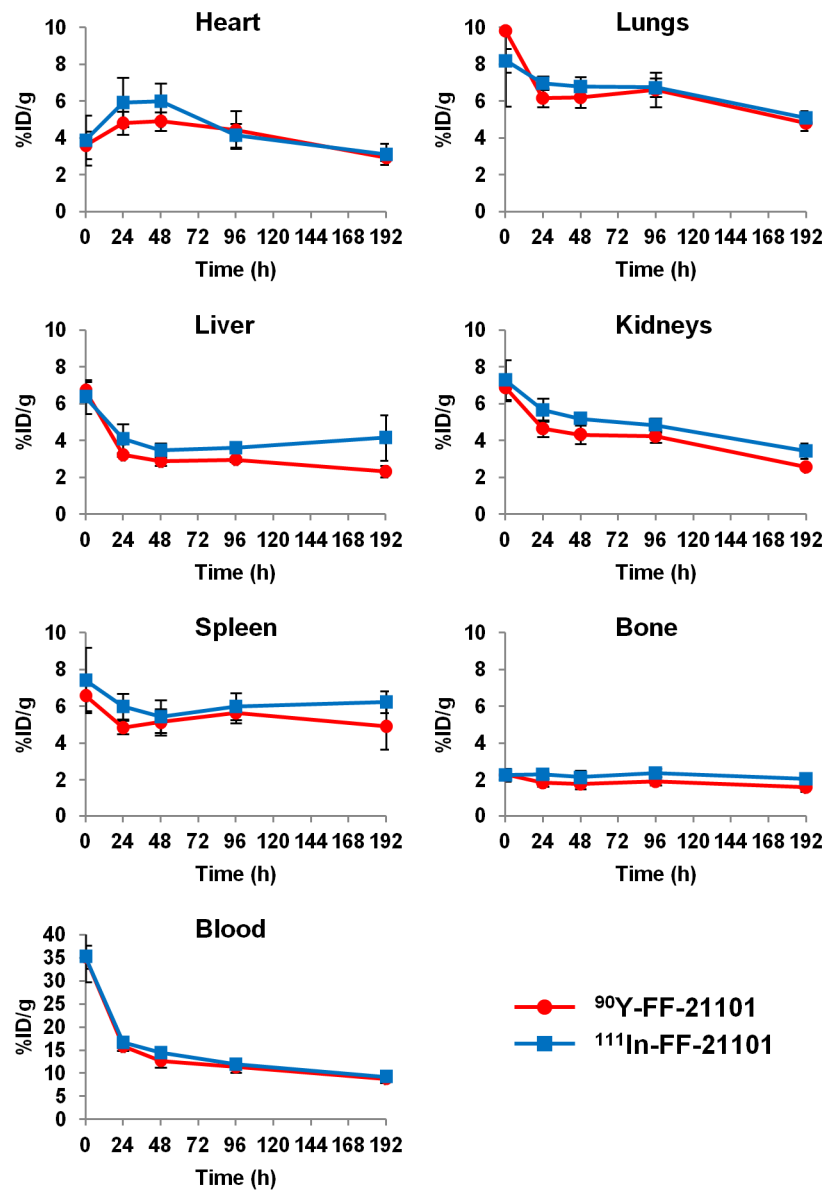
FIGURE 2. Time activity (%ID/g) curves of ^{90}Y-FF-21101 and ^{111}In-FF-21101 in each organ of normal mice

Error bars represent SD (n=3 per time point).
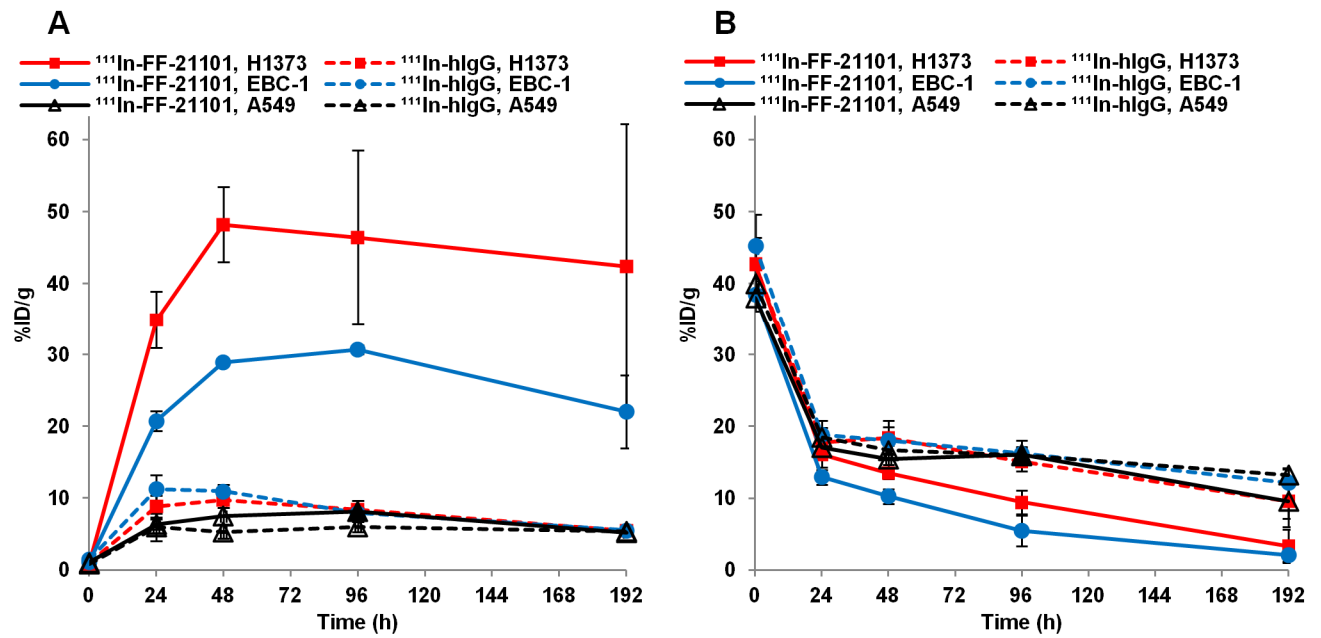
FIGURE 3. ^{111}In-FF-21101 and ^{111}In-hIgG tumor and blood uptake in high (H1373), moderate (EBC-1), and

negative (A549) P-cadherin expressing mouse xenograft models

Time activity (%ID/g) curve of tumor (A) and blood (B). Error bars represent SD (n=3 per time point).
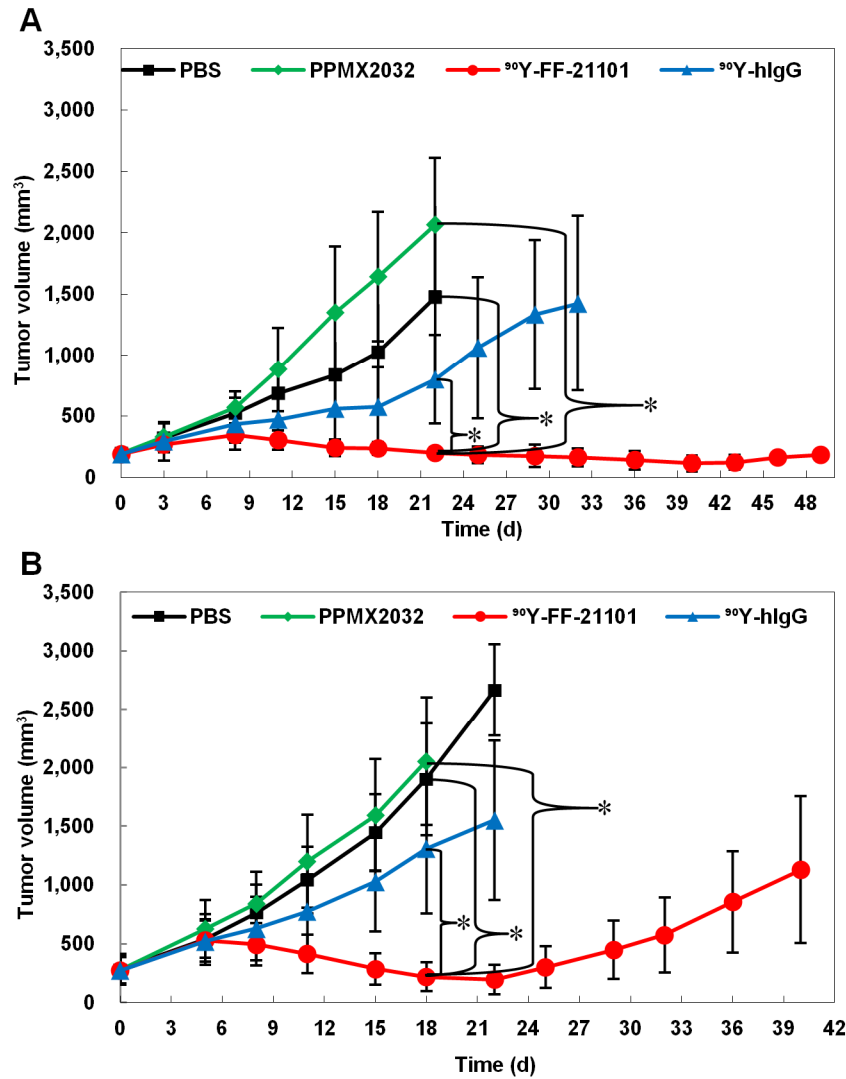
FIGURE 4. Tumor suppression in mouse xenograft models

Tumor growth curve of NCI-H1373 (A) and EBC-1 (B) mouse xenograft models. Tumor growth curves show mean tumor volumes ± SD (n=6). Curves are plotted until the first tumor per group reached 10% of the total body weight.

*P<0.05.
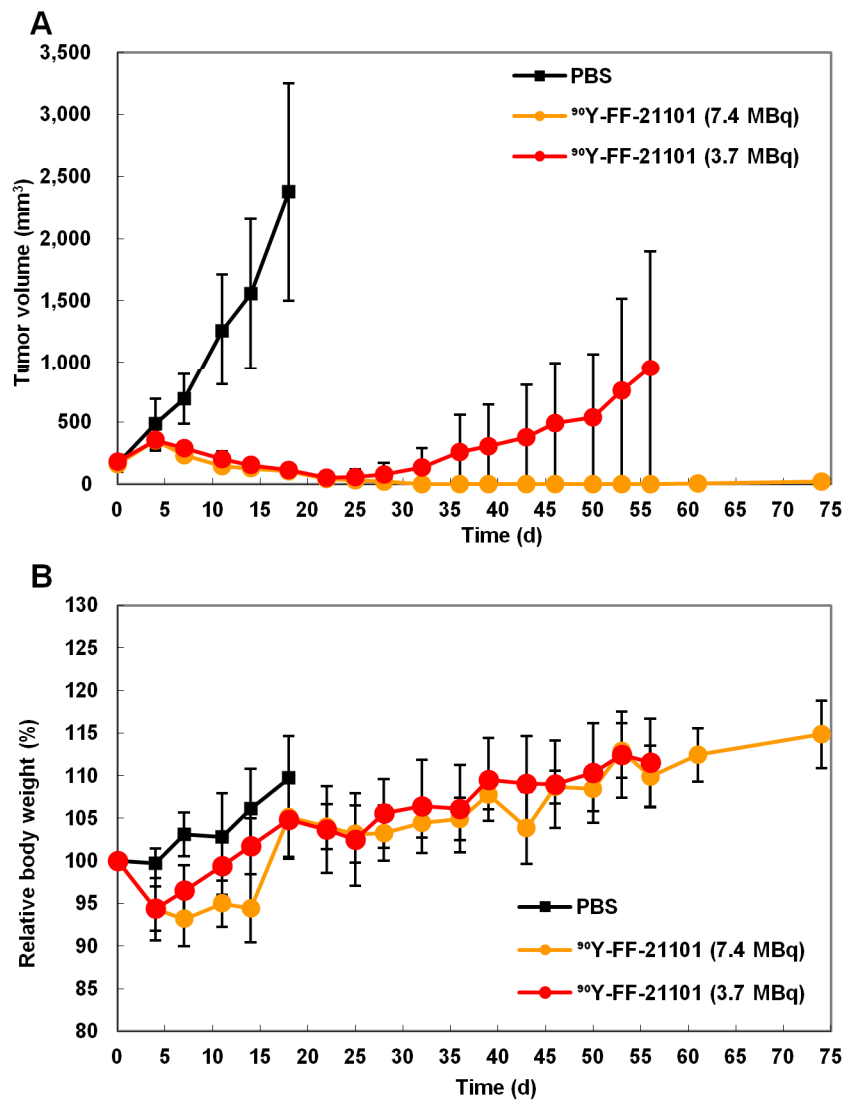
FIGURE 5. Radiation dose dependency of ^{90}Y-FF-21101 in the EBC1 mouse xenograft model

(A) Tumor growth curve. (B) Relative body weight. Curves show mean ± SD (n=6). Curves are plotted until the first

tumor per group reached 10% of the total body weight.
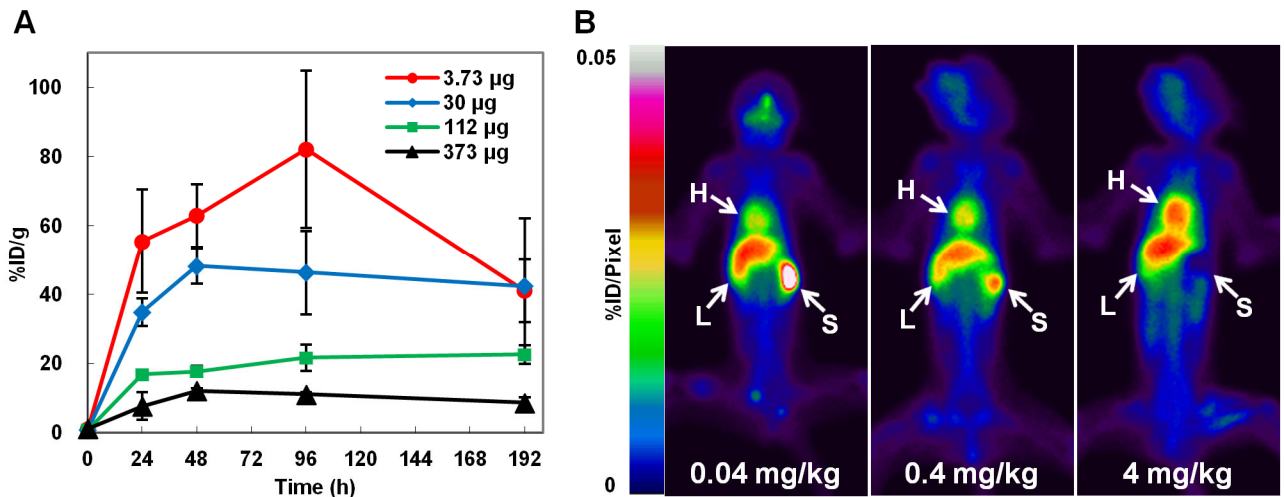
FIGURE 6. Effect of antibody dose on tumor accumulation and biodistribution

(A) Tumor accumulation for different antibody doses (3.73, 30, 112, and 373 μg/animal) of ^{111}In-FF-21101 in the

NCI-H1373 mouse xenograft model. The results are presented as %ID/g of tumor at each time point. Error bars

represent SD (n=3 per time point). (B) Whole-body planar imaging of cynomolgus monkeys 48 h after

^{111}In-FF-21101 administration. The location of the heart (H), liver (L), and spleen (S) are indicated by arrows.

Full-field-of-view images are shown in Supplemental Figures 3–5.

TABLE 1. Stability of radiolabeled FF-21101 in human serum (relative change (%) of intact)

	Incubation time			
	3 h	24 h	48 h	96 h
^{90}Y-FF-21101	96.9 ± 0.2	94.7 ± 0.3	94.3 ± 0.4	93.7 ± 0.7
^{111}In-FF-21101	99.8 ± 0.2	99.3 ± 1.5	99.3 ± 0.2	98.1 ± 1.5

Values are presented as mean $\pm$ SD (n=3).

TABLE 2. PK parameters of ^{90}Y-FF-21101 and ^{111}In-FF-21101 in normal mice

	C_{max}	AUC	$T_{1/2}$	CL	V_{ss}
	(%ID/g)	(%ID×h/g)	(h)	(g/h)	(g)
^{90}Y-FF-21101	35.32	5971.67	273.38	0.02	6.25
^{111}In-FF-21101	35.94	5733.08	231.14	0.02	5.52

TABLE 3. PK parameters calculated from blood radioactivity in ^{111}In-FF-21101 administered to cynomolgus

monkeys

	Antibody dose		
	0.04 mg/kg	0.4 mg/kg	4 mg/kg
C_{max} (%ID/mL)	0.52	0.45	0.47
AUC (%ID·h/mL)	38.75	43.26	69.32
$T_{1/2}$ (h)	147.73	147.10	241.91
CL (mL/h/kg)	0.88	0.68	0.44
V_{ss} (mL/kg)	146.93	124.61	136.14

TABLE 4. Estimated radiation-absorbed dose (mGy/MBq) of ^{90}Y-FF-21101 in humans

	Antibody dose		
	0.04 mg/kg	0.4 mg/kg	4 mg/kg
Heart wall	2.31	2.54	3.28
Liver	2.56	2.47	2.55
Lungs	1.21	1.19	1.82
Red marrow	0.661	0.786	0.885
Osteogenic cells	0.680	0.817	0.912
Spleen	12.0	6.93	2.77
Total body	0.382	0.423	0.459

TABLE 5. Antibody dose of cynomolgus monkey (mg/kg) and mouse [μg/animal (25 g)] corresponding to the

antibody dose per body surface area (mg/m^2)

	Antibody dose		
Dose per body weight [monkey (mg/kg)]	0.04	0.4	4
Dose per body surface area (mg/m^2)	0.48	4.8	48
Dose per individual [mouse (μg/animal)]	4	40	400

TABLE 6. Estimated dose-limiting organ and maximum radiation dose at each antibody dose

Antibody dose (mg/m^2)	Dose-limiting organ	Maximum radiation dose (MBq/human)
0.48	Spleen	1,667
4.8	Spleen	2,886
48	Red marrow	3,390

Maximum radiation dose calculation is shown in Supplemental Method 5 (*30*).

Supplemental information

Supplemental Method 1

<Calculation of Radioactivity Concentration for in Vitro Stability>

Radioactivity concentration was set assuming the maximum serum concentration in human

$740\ \text{MBq/m}^2 \times 1.89\ \text{m}^2 / 2836.0\ \text{mL} = 0.5\ \text{MBq/mL}$

   Putative radiation dose: $740\ \text{MBq/m}^2$

   Human body surface area: $1.89\ \text{m}^2 = \text{Height}^{0.725} \times \text{Weight}^{0.425} \times 0.007184$ (*1*)

     Height: 176 cm (*2*)

     Weight: 73 kg (*2*)

   Serum volume: $2836.0\ \text{mL} = \text{Blood volume} \times (1 - \text{Hematocrit}) \times \text{Weight}$

     Blood volume: 73.3 mL/kg (*3*)

     Hematocrit: 0.47

Supplemental Method 2

<Calculation for Dosage Based on Body Surface Area Conversion; Monkey mg/kg to mg/m^2>

   To convert dose in mg/kg to dose in mg/m^2 multiply factor (K_m) of monkey: $12\ \text{kg/m}^2$ (*4*)

   $0.04\ (\text{mg/kg}) \times 12\ (\text{kg/m}^2) = 0.48\ (\text{mg/m}^2)$

   $0.4\ (\text{mg/kg}) \times 12\ (\text{kg/m}^2) = 4.8\ (\text{mg/m}^2)$

   $4\ (\text{mg/kg}) \times 12\ (\text{kg/m}^2) = 48\ (\text{mg/m}^2)$

The mg/head of mouse corresponding to the above dosage based on body surface area was calculated.

   To convert dose in mg/kg to dose in mg/m^2 multiply factor (K_m) of mouse: $3\ \text{kg/m}^2$ (*4*)

   Mouse body weight: 0.025 kg/head

   $0.48\ (\text{mg/m}^2) / 3\ (\text{kg/m}^2) \times 0.025\ (\text{kg/head}) = 0.004\ (\text{mg/head})$

   $4.8\ (\text{mg/m}^2) / 3\ (\text{kg/m}^2) \times 0.025\ (\text{kg/head}) = 0.04\ (\text{mg/head})$

   $48\ (\text{mg/m}^2) / 3\ (\text{kg/m}^2) \times 0.025\ (\text{kg/head}) = 0.4\ (\text{mg/head})$

Supplemental Method 3

< Calculation for Dosage Based on Body Surface Area Conversion; Mouse MBq/head to MBq/m^2>

The therapeutic radiation dose (MBq/head) of mouse was converted to the dosage based on body surface area

   To convert dose in mg/kg to dose in mg/m^2 multiply factor (K_m) of mouse: $3\ \text{kg/m}^2$ (*4*)

   The Km for mg/kg was applied to MBq/kg.

   Mouse body weight: 0.025 kg/head

7.4 (MBq/head) / 0.025 (kg/head) × 3 (kg/m^2) = 888 (MBq/m^2)

Human body surface area: 1.89 m^2 = Height$^{0.725}$ × Weight$^{0.425}$ × 0.007184 (*1*)

  Height: 176 cm (*2*)

  Weight: 73 kg (*2*)

888 (MBq/m^2) ×1.89 (m^2) = 1,678 (MBq)

Supplemental Method 4

< Calculation for Dosage Based on Bodyweight Conversion; mg/m^2 to Human mg/kg>

  To convert dose in mg/kg to dose in mg/m^2 multiply factor (K$_m$) of human: 37 kg/m^2 (*4*)

  4.8 (mg/m^2) / (37 kg/m^2) = 0.13 (mg/kg)

Supplemental Method 5

<Calculation of Maximum Radiation Dose>

The upper limits of the absorbed dose were set at 3,000 mGy and 20,000 mGy for the red marrow and any other organ, respectively (*5*).

  0.04 mg/kg:

  Hat wall: 20,000 mGy / 2.31 mGy/MBq = 8,658 MBq

  Liver: 20,000 mGy / 2.56 mGy/MBq = 7,813 MBq

  Lungs: 20,000 mGy / 1.21 mGy/MBq = 16,529 MBq

  Red marrow: 3,000 mGy / 0.661 mGy/MBq = 4,539 MBq

  Osteogenic cells: 20,000 mGy / 0.680 mGy/MBq = 29,412 MBq

  Spleen: 20,000 mGy / 12.0 mGy/MBq = 1,667 MBq

  0.4 mg/kg:

  Hat wall: 20,000 mGy / 2.54 mGy/MBq = 7,874 MBq

  Liver: 20,000 mGy / 2.47 mGy/MBq = 8,097 MBq

  Lungs: 20,000 mGy / 1.19 mGy/MBq = 16,807 MBq

  Red marrow: 3,000 mGy / 0.786 mGy/MBq = 3,817 MBq

  Osteogenic cells: 20,000 mGy / 0.817 mGy/MBq = 24,480 MBq

  Spleen: 20,000 mGy / 6.93 mGy/MBq = 2,886 MBq

4 mg/kg:

Hat wall: 20,000 mGy / 3.28 mGy/MBq = 6,098 MBq

Liver: 20,000 mGy / 2.55 mGy/MBq = 7,843 MBq

Lungs: 20,000 mGy / 1.82 mGy/MBq = 10,989 MBq

Red marrow: 3,000 mGy / 0.885 mGy/MBq = 3,390 MBq

Osteogenic cells: 20,000 mGy / 0.912 mGy/MBq = 21,930 MBq

Spleen: 20,000 mGy / 2.77 mGy/MBq = 7,220 MBq

Supplemental Table 1

Tissue accumulation (%ID/g) of ^{111}In-FF-21101 in NCI-H1373 xenograft mouse model (mean ± SD)

	5min	24h	48h	96h	192h
Blood	42.758 ± 2.419	16.067 ± 1.808	13.465 ± 0.835	9.427 ± 1.673	3.309 ± 2.309
Brain	0.759 ± 0.090	0.333 ± 0.034	0.287 ± 0.037	0.219 ± 0.024	0.096 ± 0.053
Heart	5.383 ± 0.588	3.913 ± 0.666	3.636 ± 0.594	2.859 ± 0.239	1.172 ± 0.424
Lungs	10.515 ± 2.618	6.145 ± 0.683	5.078 ± 0.772	4.216 ± 0.660	1.687 ± 0.944
Liver	7.022 ± 0.488	4.828 ± 1.023	4.286 ± 0.438	3.843 ± 0.326	2.859 ± 0.771
Spleen	6.277 ± 0.365	4.460 ± 0.678	4.447 ± 0.368	4.231 ± 0.328	3.113 ± 0.620
Pancreas	1.302 ± 0.342	1.475 ± 0.200	1.271 ± 0.092	0.984 ± 0.131	0.471 ± 0.188
Stomach	0.858 ± 0.101	1.648 ± 0.392	0.919 ± 0.266	0.970 ± 0.330	0.310 ± 0.103
Small-Int.	1.038 ± 0.177	1.861 ± 0.545	1.385 ± 0.327	1.086 ± 0.017	0.446 ± 0.157
Cecum	0.322 ± 0.078	1.398 ± 0.458	0.808 ± 0.194	0.818 ± 0.142	0.375 ± 0.081
Large-Int.	1.186 ± 0.834	1.753 ± 0.400	1.153 ± 0.106	1.160 ± 0.130	0.453 ± 0.170
Kidneys	7.623 ± 0.936	6.295 ± 0.970	4.977 ± 1.013	4.086 ± 0.184	2.172 ± 0.856
Adrenals	5.200 ± 2.422	3.105 ± 0.889	2.530 ± 0.416	1.983 ± 0.551	1.018 ± 0.200
Adipose	0.790 ± 0.243	1.508 ± 0.532	0.984 ± 0.078	0.639 ± 0.243	0.380 ± 0.162
Testes	0.932 ± 0.186	2.521 ± 0.102	2.257 ± 0.356	2.242 ± 0.236	1.582 ± 0.377
Bone	2.271 ± 0.141	1.747 ± 0.244	1.729 ± 0.039	1.525 ± 0.160	0.883 ± 0.400
Muscle	0.455 ± 0.049	0.943 ± 0.129	1.020 ± 0.204	0.680 ± 0.083	0.290 ± 0.120
Skin	0.927 ± 0.188	5.362 ± 0.732	4.214 ± 0.673	3.834 ± 0.376	1.846 ± 0.027
Tumor	0.852 ± 0.036	34.914 ± 3.962	48.222 ± 5.198	46.398 ± 12.177	42.428 ± 19.80

Supplemental Table 2

Tissue accumulation (%ID/g) of ^{111}In-FF-21101 in EBC-1 xenograft mouse model (mean ± SD)

	5min	24h	48h	96h	192h
Blood	38.459 ± 2.307	12.936 ± 1.015	10.251 ± 1.022	5.464 ± 2.164	2.078 ± 0.884
Brain	0.739 ± 0.123	0.588 ± 0.517	0.248 ± 0.040	0.131 ± 0.090	0.068 ± 0.021
Heart	5.298 ± 1.222	2.763 ± 1.642	3.000 ± 0.680	1.743 ± 0.751	0.818 ± 0.292
Lungs	9.670 ± 0.861	4.409 ± 0.657	3.888 ± 0.301	2.580 ± 0.856	1.223 ± 0.405
Liver	6.831 ± 1.350	4.965 ± 1.152	3.563 ± 0.403	3.086 ± 0.983	2.471 ± 0.608
Spleen	5.302 ± 1.129	3.715 ± 2.021	4.350 ± 0.848	3.101 ± 0.718	2.993 ± 0.937
Pancreas	1.211 ± 0.193	1.597 ± 0.512	1.039 ± 0.081	0.679 ± 0.110	0.385 ± 0.127
Stomach	0.793 ± 0.319	1.125 ± 0.359	0.750 ± 0.145	0.503 ± 0.169	0.260 ± 0.110
Small-Int.	1.006 ± 0.120	1.305 ± 0.090	1.141 ± 0.143	0.721 ± 0.179	0.331 ± 0.125
Cecum	0.328 ± 0.158	0.989 ± 0.179	0.770 ± 0.019	0.708 ± 0.182	0.303 ± 0.068
Large-Int.	0.898 ± 0.459	1.213 ± 0.231	1.033 ± 0.067	0.754 ± 0.203	0.361 ± 0.078
Kidneys	6.977 ± 0.209	5.480 ± 0.516	4.732 ± 0.569	3.347 ± 0.340	1.805 ± 0.429
Adrenals	4.098 ± 0.896	2.121 ± 0.424	2.023 ± 0.332	1.112 ± 0.422	0.672 ± 0.128
Adipose	0.868 ± 0.128	0.928 ± 0.269	0.638 ± 0.055	0.536 ± 0.175	0.262 ± 0.096
Testes	0.737 ± 0.085	2.265 ± 0.236	1.687 ± 0.173	1.272 ± 0.567	1.162 ± 0.274
Bone	1.913 ± 0.221	1.622 ± 0.376	1.479 ± 0.159	1.016 ± 0.169	0.677 ± 0.279
Muscle	0.423 ± 0.049	0.924 ± 0.169	0.846 ± 0.094	0.808 ± 0.426	0.199 ± 0.039
Skin	0.844 ± 0.371	5.467 ± 0.540	4.282 ± 0.194	2.473 ± 0.432	1.410 ± 0.268
Tumor	1.061 ± 0.080	20.752 ± 1.407	28.936 ± 0.274	30.688 ± 0.650	22.026 ± 5.079

Supplemental Table 3

Tissue accumulation (%ID/g) of ^{111}In-FF-21101 in A549 xenograft mouse model (mean ± SD)

	5min	24h	48h	96h	192h
Blood	37.997 ± 1.216	17.084 ± 0.301	15.451 ± 0.781	16.027 ± 0.945	9.558 ± 2.434
Brain	0.861 ± 0.068	0.400 ± 0.048	0.393 ± 0.052	0.370 ± 0.026	0.266 ± 0.056
Heart	4.657 ± 1.285	4.657 ± 0.623	4.367 ± 0.824	4.158 ± 0.205	2.764 ± 0.758
Lungs	11.610 ± 1.107	5.719 ± 0.597	6.211 ± 0.505	6.220 ± 0.467	4.399 ± 1.006
Liver	6.750 ± 0.173	4.656 ± 0.447	5.769 ± 1.151	4.753 ± 1.354	4.768 ± 0.851
Spleen	6.843 ± 0.369	6.080 ± 1.727	5.977 ± 1.318	7.219 ± 1.329	4.690 ± 1.029
Pancreas	1.056 ± 0.156	1.188 ± 0.028	1.325 ± 0.085	1.559 ± 0.104	1.016 ± 0.267
Stomach	0.657 ± 0.190	1.494 ± 0.211	1.150 ± 0.091	1.346 ± 0.049	0.993 ± 0.405
Small-Int.	0.912 ± 0.214	1.455 ± 0.042	1.665 ± 0.076	1.662 ± 0.242	1.161 ± 0.372
Cecum	0.333 ± 0.021	0.936 ± 0.127	1.223 ± 0.177	1.152 ± 0.284	0.678 ± 0.124
Large-Int.	0.848 ± 0.171	1.192 ± 0.190	1.718 ± 0.084	1.513 ± 0.270	0.962 ± 0.182
Kidneys	8.473 ± 1.551	4.474 ± 0.460	4.612 ± 0.410	4.733 ± 0.434	3.437 ± 1.010
Adrenals	4.685 ± 3.032	3.028 ± 0.905	3.006 ± 0.166	2.903 ± 0.273	2.269 ± 0.807
Adipose	0.849 ± 0.120	1.082 ± 0.112	1.317 ± 0.301	1.084 ± 0.257	0.832 ± 0.254
Testes	0.760 ± 0.143	2.807 ± 0.167	2.921 ± 0.267	3.161 ± 0.369	2.673 ± 0.456
Bone	2.575 ± 0.094	1.769 ± 0.246	1.922 ± 0.195	2.468 ± 0.225	1.610 ± 0.353
Muscle	0.544 ± 0.004	1.098 ± 0.099	1.256 ± 0.059	1.154 ± 0.149	0.785 ± 0.218
Skin	1.117 ± 0.294	4.468 ± 0.149	6.479 ± 1.081	5.416 ± 0.288	3.613 ± 0.418
Tumor	1.030 ± 0.055	6.347 ± 0.679	7.482 ± 1.157	8.120 ± 0.198	5.200 ± 0.194

Supplemental Table 4

Tissue accumulation (%ID/g) of ^{111}In-hIgG in NCI-H1373 xenograft mouse model (mean ± SD)

	5min	24h	48h	96h	192h
Blood	42.704 ± 3.745	17.800 ± 0.904	18.417 ± 2.365	15.096 ± 1.340	9.585 ± 3.631
Brain	0.852 ± 0.039	0.404 ± 0.027	0.391 ± 0.052	0.332 ± 0.040	0.214 ± 0.084
Heart	6.262 ± 1.060	5.417 ± 1.196	4.637 ± 0.499	3.933 ± 0.443	2.698 ± 1.051
Lungs	11.594 ± 1.236	7.140 ± 0.872	6.474 ± 0.897	6.605 ± 0.653	4.366 ± 1.289
Liver	8.464 ± 2.029	5.630 ± 1.134	5.062 ± 0.515	5.430 ± 1.429	4.561 ± 0.553
Spleen	8.735 ± 3.571	4.360 ± 0.327	4.984 ± 0.637	5.529 ± 1.240	4.041 ± 1.061
Pancreas	1.644 ± 0.293	1.486 ± 0.320	1.491 ± 0.168	1.327 ± 0.016	1.110 ± 0.325
Stomach	1.134 ± 0.124	1.472 ± 0.377	1.240 ± 0.313	1.234 ± 0.259	1.171 ± 0.038
Small-Int.	1.171 ± 0.346	1.833 ± 0.175	1.691 ± 0.201	1.645 ± 0.089	1.142 ± 0.315
Cecum	0.313 ± 0.048	1.469 ± 0.276	1.141 ± 0.073	1.142 ± 0.124	0.692 ± 0.104
Large-Int.	0.967 ± 0.084	1.874 ± 0.297	1.642 ± 0.202	1.446 ± 0.056	1.088 ± 0.244
Kidneys	8.076 ± 1.851	7.138 ± 1.302	6.184 ± 0.360	5.249 ± 0.196	3.588 ± 0.981
Adrenals	6.136 ± 0.295	3.191 ± 0.172	3.042 ± 1.126	2.968 ± 0.120	2.765 ± 0.754
Adipose	0.943 ± 0.048	1.020 ± 0.118	1.005 ± 0.333	1.113 ± 0.134	0.999 ± 0.470
Testes	0.815 ± 0.179	2.941 ± 0.174	3.100 ± 0.066	3.079 ± 0.641	2.893 ± 0.478
Bone	2.223 ± 0.491	1.832 ± 0.120	1.897 ± 0.446	1.887 ± 0.293	1.467 ± 0.632
Muscle	0.373 ± 0.049	1.363 ± 0.263	1.261 ± 0.010	1.004 ± 0.186	0.760 ± 0.250
Skin	1.230 ± 0.440	4.894 ± 0.212	4.480 ± 0.138	4.416 ± 0.380	3.709 ± 0.573
Tumor	0.991 ± 0.075	8.847 ± 1.490	9.709 ± 0.023	8.365 ± 1.267	5.459 ± 0.335

Supplemental Table 5

Tissue accumulation (%ID/g) of ^{111}In-hIgG in EBC-1 xenograft mouse model (mean ± SD)

|	5min	24h	48h	96h	192h
Blood	45.249 ± 4.358	18.859 ± 1.898	18.049 ± 0.773	16.221 ± 1.819	12.188 ± 1.859
Brain	0.981 ± 0.109	0.430 ± 0.074	0.406 ± 0.036	0.351 ± 0.053	0.267 ± 0.020
Heart	5.766 ± 1.820	4.849 ± 0.651	4.317 ± 0.558	2.270 ± 1.264	2.718 ± 0.398
Lungs	11.832 ± 1.139	6.821 ± 0.332	6.875 ± 0.751	5.738 ± 0.533	5.152 ± 0.345
Liver	8.860 ± 0.414	5.725 ± 0.064	4.950 ± 0.824	4.197 ± 0.314	4.417 ± 1.706
Spleen	7.913 ± 1.741	4.539 ± 0.458	5.099 ± 0.771	5.803 ± 1.449	5.538 ± 0.692
Pancreas	1.415 ± 0.329	1.407 ± 0.148	1.457 ± 0.271	1.383 ± 0.138	1.078 ± 0.163
Stomach	0.764 ± 0.294	1.152 ± 0.414	1.096 ± 0.195	1.212 ± 0.241	1.003 ± 0.474
Small-Int.	1.041 ± 0.258	1.614 ± 0.293	1.451 ± 0.122	1.527 ± 0.094	1.157 ± 0.366
Cecum	0.330 ± 0.079	1.144 ± 0.152	0.922 ± 0.008	0.932 ± 0.102	0.852 ± 0.016
Large-Int.	0.691 ± 0.111	1.545 ± 0.284	1.410 ± 0.207	1.271 ± 0.244	1.107 ± 0.137
Kidneys	7.967 ± 2.198	6.680 ± 1.235	6.749 ± 0.837	5.871 ± 0.295	3.867 ± 0.508
Adrenals	4.602 ± 0.674	3.293 ± 0.270	2.814 ± 0.284	2.881 ± 0.108	2.419 ± 0.642
Adipose	0.832 ± 0.125	1.026 ± 0.103	0.910 ± 0.211	1.100 ± 0.005	0.906 ± 0.052
Testes	0.754 ± 0.094	3.316 ± 0.346	3.175 ± 0.529	2.896 ± 0.327	2.783 ± 0.163
Bone	2.499 ± 0.456	1.801 ± 0.290	1.923 ± 0.106	1.672 ± 0.072	1.847 ± 0.186
Muscle	0.451 ± 0.067	1.201 ± 0.197	1.357 ± 0.304	1.171 ± 0.162	0.821 ± 0.058
Skin	0.995 ± 0.196	5.604 ± 0.318	5.499 ± 0.635	5.032 ± 0.398	4.147 ± 0.113
Tumor	1.425 ± 0.175	11.278 ± 1.999	10.946 ± 2.354	7.908 ± 1.090	5.501 ± 0.881

Supplemental Table 6

Tissue accumulation (%ID/g) of ^{111}In-hIgG in A549 xenograft mouse model (mean ± SD)

	5min	24h	48h	96h	192h
Blood	39.980 ± 3.194	18.477 ± 1.355	16.656 ± 3.269	15.947 ± 1.178	13.193 ± 0.974
Brain	0.664 ± 0.051	0.347 ± 0.060	0.336 ± 0.070	0.347 ± 0.010	0.307 ± 0.077
Heart	4.533 ± 1.500	4.655 ± 1.160	4.709 ± 1.323	3.915 ± 0.411	3.402 ± 0.414
Lungs	9.031 ± 1.245	6.748 ± 1.736	5.724 ± 0.589	6.574 ± 0.827	5.975 ± 0.462
Liver	7.949 ± 0.847	5.131 ± 0.664	5.044 ± 0.635	5.364 ± 1.674	4.189 ± 0.408
Spleen	7.949 ± 2.641	6.312 ± 2.043	5.277 ± 1.136	5.837 ± 0.505	5.971 ± 0.829
Pancreas	1.058 ± 0.109	1.359 ± 0.361	1.386 ± 0.140	1.269 ± 0.115	1.237 ± 0.195
Stomach	0.796 ± 0.105	1.508 ± 0.702	1.109 ± 0.326	1.363 ± 0.214	0.647 ± 0.056
Small-Int.	0.881 ± 0.104	1.535 ± 0.134	1.668 ± 0.160	1.448 ± 0.180	1.165 ± 0.056
Cecum	0.323 ± 0.044	1.118 ± 0.344	1.330 ± 0.334	0.957 ± 0.020	0.775 ± 0.059
Large-Int.	0.660 ± 0.051	1.499 ± 0.716	1.569 ± 0.338	1.486 ± 0.267	1.074 ± 0.054
Kidneys	7.949 ± 0.890	6.975 ± 1.294	6.067 ± 1.112	5.313 ± 0.483	4.353 ± 0.557
Adrenals	4.697 ± 0.615	2.631 ± 0.598	3.259 ± 0.406	3.028 ± 0.740	3.251 ± 0.706
Adipose	1.108 ± 0.198	1.035 ± 0.138	1.774 ± 0.161	1.079 ± 0.113	1.084 ± 0.175
Testes	0.800 ± 0.075	2.860 ± 0.500	2.747 ± 0.598	3.390 ± 0.729	3.131 ± 0.261
Bone	2.317 ± 0.164	2.006 ± 0.477	1.995 ± 0.311	2.093 ± 0.271	1.951 ± 0.161
Muscle	0.469 ± 0.053	1.064 ± 0.072	1.174 ± 0.245	1.023 ± 0.063	0.936 ± 0.092
Skin	1.224 ± 0.608	5.455 ± 1.846	6.472 ± 2.032	5.288 ± 0.477	3.750 ± 0.449
Tumor	0.816 ± 0.121	5.966 ± 1.924	5.302 ± 0.921	5.989 ± 0.732	5.351 ± 0.451

Supplemental Figure 1

Relative body weight (%) of EBC-1 xenograft mouse model in treatment study

(□: PBS, ■: PPMX2032, ▲: ^{90}Y-hIgG, ●: ^{90}Y-FF-21101)
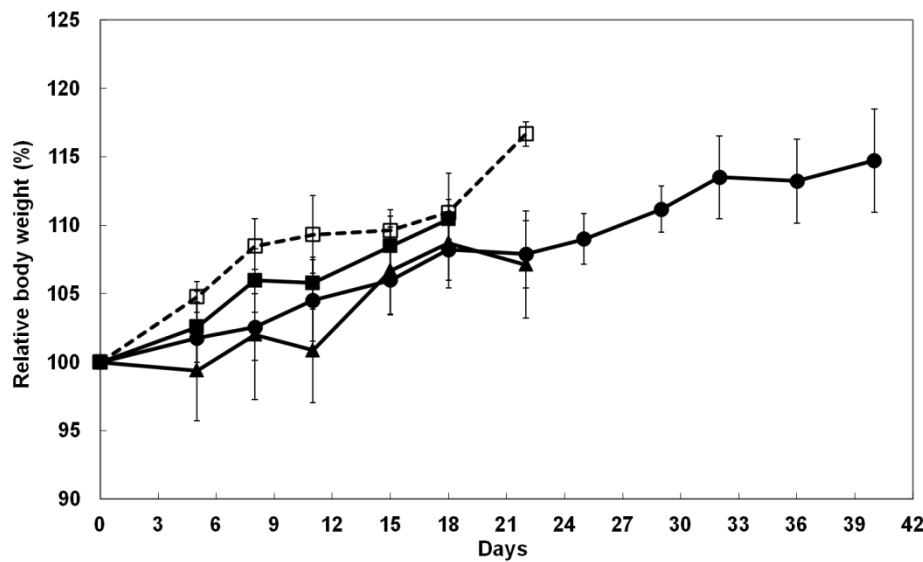

Supplemental Figure 2

Relative body weight (%) of NCI-H1373 xenograft mouse model in treatment study

(□: PBS, ■: PPMX2032, ▲: ^{90}Y-hIgG, ●: ^{90}Y-FF-21101)
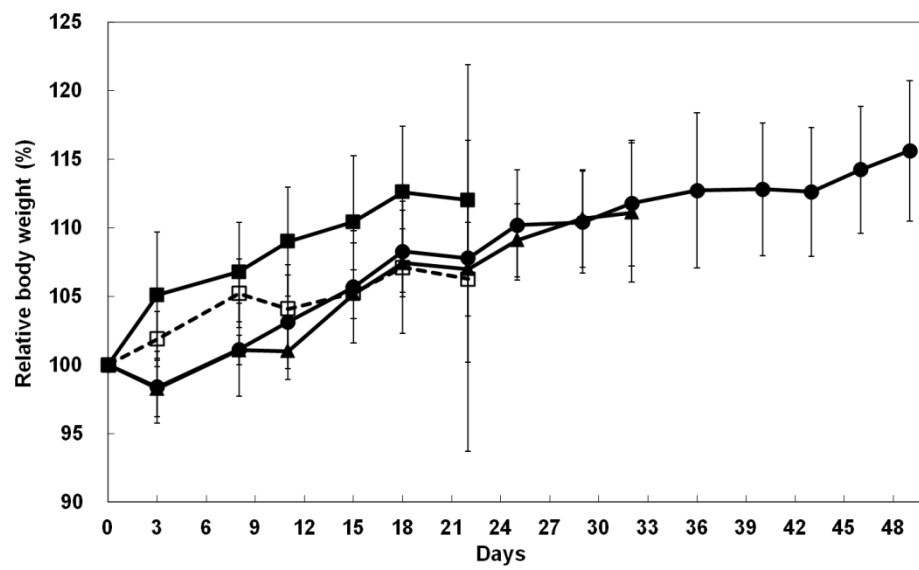
Supplemental Figure 3

Full-field-of-view image of planar imaging of cynomorgus monkey (0.04 mg/kg) 48 h after administration
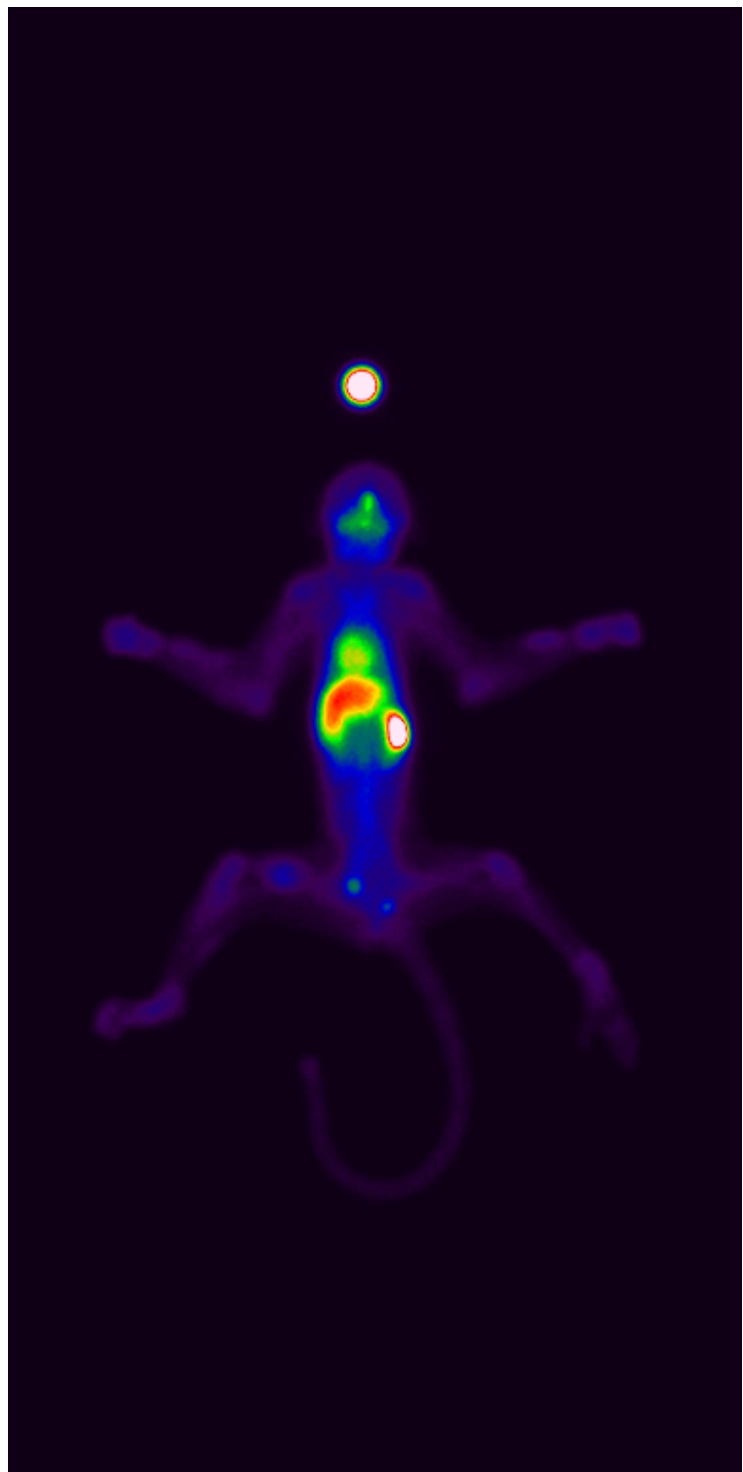
Supplemental Figure 4

Full-field-of-view image of planar imaging of cynomorgus monkey (0.4 mg/kg) 48 h after administration
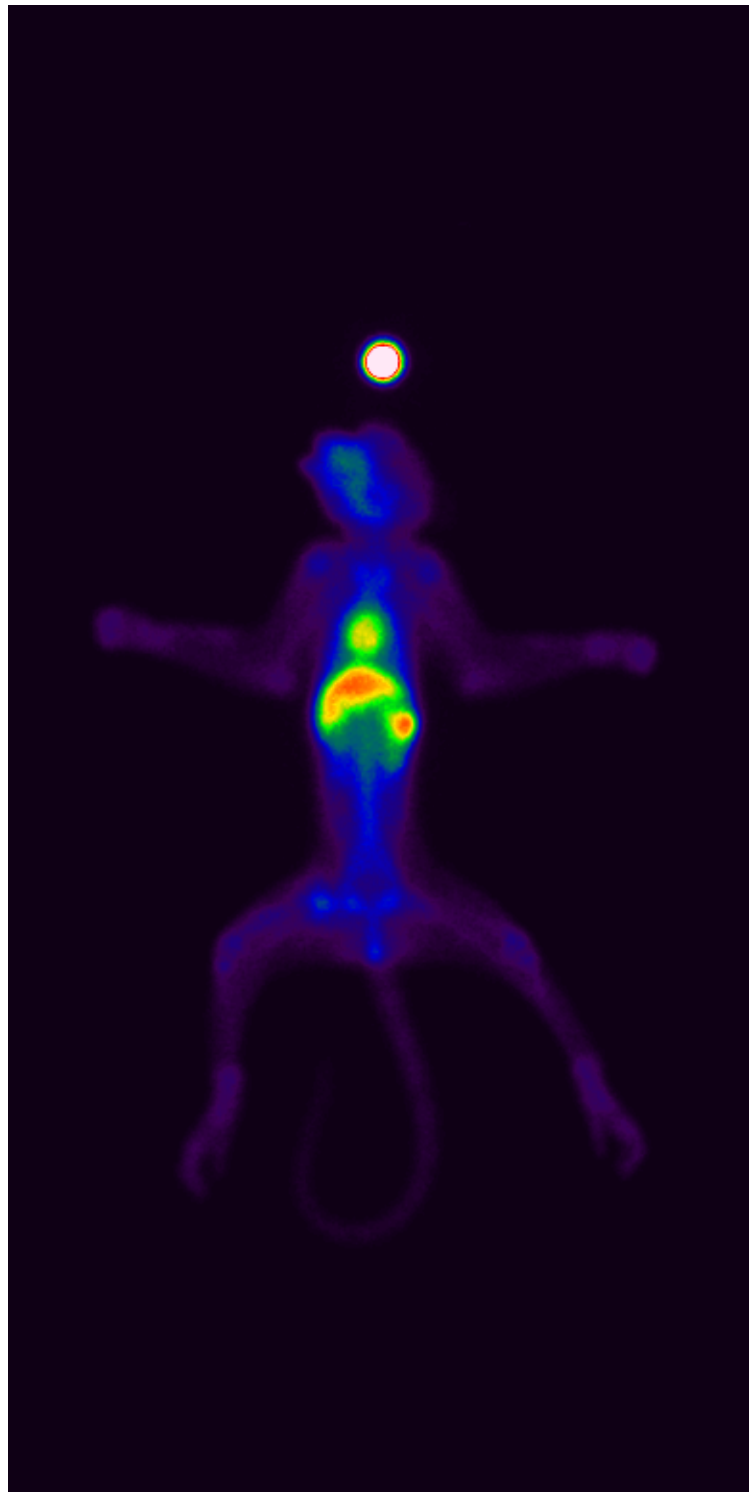
Supplemental Figure 5

Full-field-of-view image of planar imaging of cynomorgus monkey (4 mg/kg) 48 h after administration

Reference for Supplemental Information

1.   Du Bois D, Du Bois EF. A formula to estimate the approximate surface area if height and weight be known. 1916. *Nutrition.* 1989;5:303-311; discussion 312-303.

2.   Protection ICoR. Basic Anatomical and Physiological Data for Use in Radiological Protection Reference Values. *ICRP Publication 89.* 2002;32:5-265.

3.   Feldschuh J, Enson Y. Prediction of the normal blood volume. Relation of blood volume to body habitus. *Circulation.* 1977;56:605-612.

4.   Nair AB, Jacob S. A simple practice guide for dose conversion between animals and human. *J Basic Clin Pharm.* 2016;7:27-31.

5.   Wiseman GA, White CA, Sparks RB, et al. Biodistribution and dosimetry results from a phase III prospectively randomized controlled trial of Zevalin radioimmunotherapy for low-grade, follicular, or transformed B-cell non-Hodgkin's lymphoma. *Crit Rev Oncol Hematol.* 2001;39:181-194.